



Medical Imaging for Three-Dimensional Computer-Aided Models

Paulo Henrique Junqueira Amorim, Thiago Franco de Moraes, Rodrigo Alvarenga Rezende, Jorge Vicente Lopes da Silva, and Helio Pedrini

Contents

1	Introduction	196
2	Medical Image Acquisition	196
2.1	Imaging Techniques	196
2.2	DICOM Format	199
3	Preprocessing	200
3.1	Noise Filtering	200
3.2	Edge Detection	201
3.3	Contrast Enhancement	203
4	Segmentation	205
4.1	Thresholding	205
4.2	Region Growing	205
4.3	Watershed	206
5	Registration	206
6	Volume Rendering	207
6.1	Isosurface Rendering	207
6.2	Direct Volume Rendering	208
7	3D Printing and Biofabrication	211
8	Conclusions	218
	References	218

P. H. Junqueira Amorim (✉) · T. F. de Moraes · R. A. Rezende · J. V. L. da Silva
Division of 3D Technologies, Center for Information Technology Renato Archer, Campinas, SP,
Brazil
e-mail: paulo.amorim@cti.gov.br; thiago.moraes@cti.gov.br; rodrigo.rezende@cti.gov.br;
jorge.silva@cti.gov.br

H. Pedrini
Institute of Computing, University of Campinas, Campinas, SP, Brazil
e-mail: helio@ic.unicamp.br

Abstract

Technological advances in medical imaging have provided healthcare professionals with powerful resources for storing, analyzing, and visualizing three-dimensional images in a variety of diagnostic tasks. Equipments for acquiring high-quality images and computer-aided tools for image interpretation play an important role in surgical planning, disease assessment, and therapy response monitoring. This chapter presents an overview of relevant aspects related to image processing and computer graphics techniques for the construction of three-dimensional models for visualization and biofabrication.

1 Introduction

Imaging techniques have been extensively used for diagnosis in many medical specialties, whose main purpose is to create visual representations of the interior of human body. Internal anatomic structures of the body can be revealed, providing physicians with valuable clinical information about patient's conditions. Technological advances in medical imaging have aided the comprehension of structures and functions of organs, as well as the detection of abnormalities.

Several medical imaging modalities (Macovski 1983) are currently available for medical diagnosis, such as computed tomography, magnetic resonance imaging, ultrasonography, mammography, photon emission tomography, among others.

Among the various tools available for medical applications, InVesalius (Amorim et al. 2015) is an open-source framework with several functionalities for processing, analysis, visualization, and 3D printing support for medical images.

This chapter focuses on relevant image processing and computer graphics techniques for the generation of three-dimensional (3D) models for visualization and bioprinting.

In the following sections, we will describe some relevant aspects of medical imaging, preprocessing, segmentation, registration, volume rendering, 3D printing, and biofabrication.

2 Medical Image Acquisition

This section briefly describes (i) some medical imaging modalities used for diagnostic purposes and (ii) DICOM standard.

2.1 Imaging Techniques

Medical imaging is one of the most common noninvasive techniques for acquiring and interpreting images for medical diagnosis purpose. Images of internal structures

of the body can be generated and analyzed to provide a visual representation of organs and tissues.

Three-dimensional visualization of anatomic structures allow for more accurate surgical planning, reducing interventions and patient's risk.

Several imaging modalities have been developed to assist clinicians in diagnosis and treatment of patients, making beneficial impacts on healthcare. Imaging technologies currently available include computed tomography, magnetic resonance imaging, ultrasound, positron emission tomography, among others.

Computed tomography (CT) uses X-ray images acquired from different orientation angles to generate cross-sectional images around specific areas of a patient. The attenuation coefficients measured by the CT equipment are organized into a two-dimensional sinogram (Leondes 2005). Image processing and computer graphics techniques are used to produce a three-dimensional image from a sequence of two-dimensional slices (radiographic images), known as reconstruction process (Fig. 1).

Each pixel of the reconstructed image is represented in the Hounsfield unit (HU) scale. The HU value for a voxel with average linear attenuation coefficient μ is given by

$$HU = 1000 \times \frac{\mu - \mu_{\text{water}}}{\mu_{\text{water}} - \mu_{\text{air}}} \quad (1)$$

where μ_{air} and μ_{water} are the linear attenuation coefficients of air and water, respectively. In this scale, water is represented by 0, air by -1000 , and more dense bones are represented by 3000 HU (Hsieh 2003).

Typical applications of CT include the detection of brain tumors, visualization of blood vessel defects, and differentiation of soft tissues, among others. There are some variations of computed tomography such as positron emission tomography (PET-CT) used to diagnose certain tumors (Wahl and Wagner 2009) and cone beam tomography (CBCT) used in dentistry (Kapila 2014).

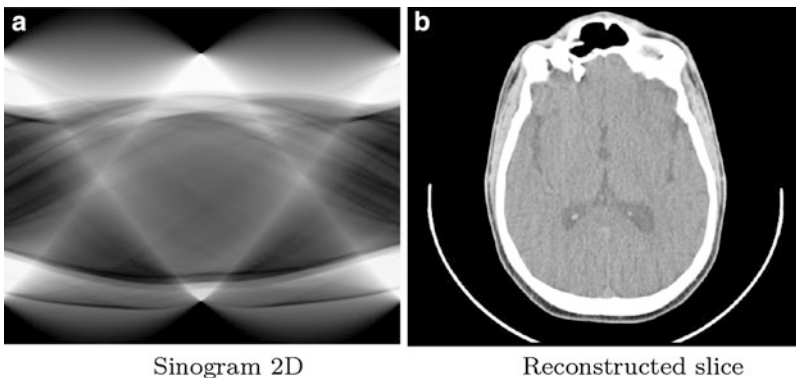


Fig. 1 Example of sinogram 2D and reconstructed image

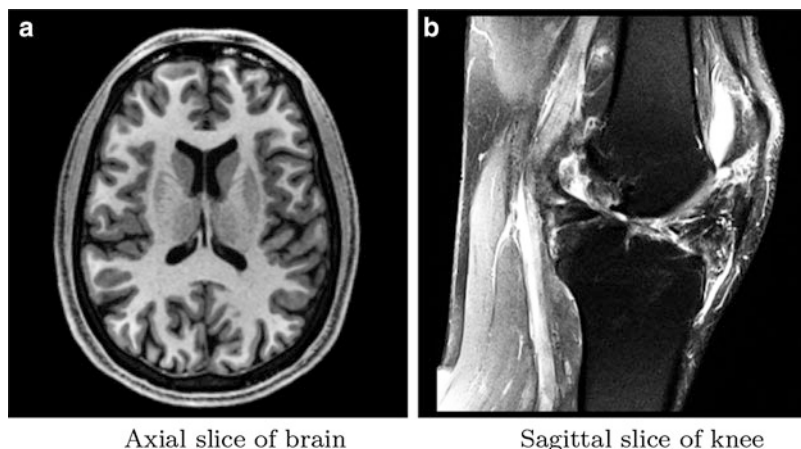


Fig. 2 Examples of MRI images

Magnetic resonance imaging (MRI) is another medical imaging technique used in radiology for diagnosis and treatment purposes.

MRI scanners employ strong magnetic fields to align the nuclei of hydrogen atoms (proton) and apply radio frequency pulses in the region under analysis to create a resonance in the proton atoms (Kelsey et al. 2013). When the radio frequency pulse is turned off, the protons align again to the magnetic field, releasing energy that is recorded by the MRI equipment. Signals at different frequencies are used to reconstruct an image.

Advantages of the MRI include its absence of ionizing radiation and capacity of providing detailed images of soft tissues (for instance, in brain and spine examination). Disadvantages include the cost of equipments compared to other modalities (Sistrom and McKay 2005), as well as counter-indication in patients with metallic devices (pacemakers, orthopedic implants) or who are claustrophobic. Figure 2 shows some examples of MRI images.

Ultrasonography is a diagnostic imaging technique that employs sound waves to form images. This technique allows the visualization of internal structures of the body such as muscles, joints, tendons, blood vessels, liver, and heart. Ultrasonography is also widely used in examination of pregnant women to evaluate the development of the fetus.

As shown in Fig. 3, a transducer converts electrical current into sound waves with frequencies between 3 and 30 MHz (Lutz et al. 2011), which are sent into the body tissues. These frequencies are higher than those audible to humans (>20 KHz). The waves are echoed off the internal structures and reflected back to the transducer, which converts the waves into electrical signals. Then, a computer converts the electrical signal patterns into an image (Dowsett et al. 2006).

Ultrasonography has several advantages compared to other medical imaging techniques. It can provide real-time images, the equipments are portable and lower

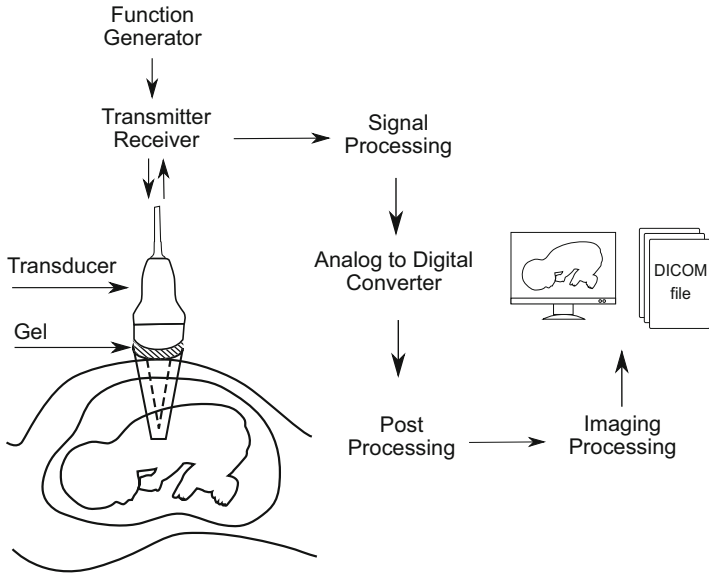


Fig. 3 Main components of an ultrasound system

Fig. 4 Example of a 2D ultrasound image



in cost, and it does not use ionizing radiation. Disadvantages include certain limitations in terms of its field of view, noise, and difficulties in visualizing structures behind air and bones. Figure 4 shows a 2D ultrasound image.

2.2 DICOM Format

Until the early 1980s, the examinations based on medical imaging were printed on X-ray film or paper in the case of ultrasonography. Many practices and specifications

were generated by a variety of manufacturers, causing serious problems in terms of data management and connectivity incompatibilities (Oosterwijk and Gihring 2002). With the development of advanced imaging techniques and availability of computers, manufacturers started storing medical images in digital format, however, in their own proprietary format.

Digital Imaging and Communications in Medicine (DICOM) (Pianykh 2009) is a standard for storing, printing, and transmitting information in medical imaging. The first version of the standard was released by American College of Radiology (ACR) and National Electrical Manufacturers Association (NEMA) in 1985. The second and third versions were released in 1988 and 1993, respectively.

DICOM provides a file format definition and a network communication protocol based on the Transmission Control Protocol/Internet Protocol (TCP/IP) (Stallings 2005). DICOM enables the integration of different equipments, such as scanners, computers, printers, and servers from different manufacturers, such that files can be exchanged among heterogeneous devices capable of recognizing patient images and data in DICOM format. DICOM standard has been widely adopted by hospitals, medical offices, and dental clinics.

3 Preprocessing

The preprocessing step concerns the techniques for enhancing characteristics of the image, before its use in subsequent tasks such as segmentation and recognition. The preprocessing includes noise filtering, contrast enhancement, and edge detection.

3.1 Noise Filtering

Noise is a random variation in color or brightness of the image, but not present in the physical objects of the scene. Noise usually occurs during the image acquisition process, and it is an undesirable artifact and may decrease the efficiency of segmentation, registration, and classification stages. As desirable characteristic, a smoothing filter, should reduce the occurrence of noise while preserving the edges of an image, since they are important visual features.

Several techniques have been proposed to filter images with the purpose of reducing noise effect. Pixel or voxel values are modified by taking into account intensity values over a neighborhood.

Mean filtering (Gonzalez and Woods 2002; Parker 2010; Russ 2015) is a simple method for smoothing images, where each pixel or voxel intensity value of the image is replaced with the average value of its neighbors. Mean filtering can be performed through a convolution operation with a kernel of adequate shape and size.

Median filtering (Gonzalez and Woods 2002; Parker 2010; Russ 2015) replaces the pixel or voxel intensity value of the image with the median of the neighboring values. The median filtering is more robust than the mean filtering since

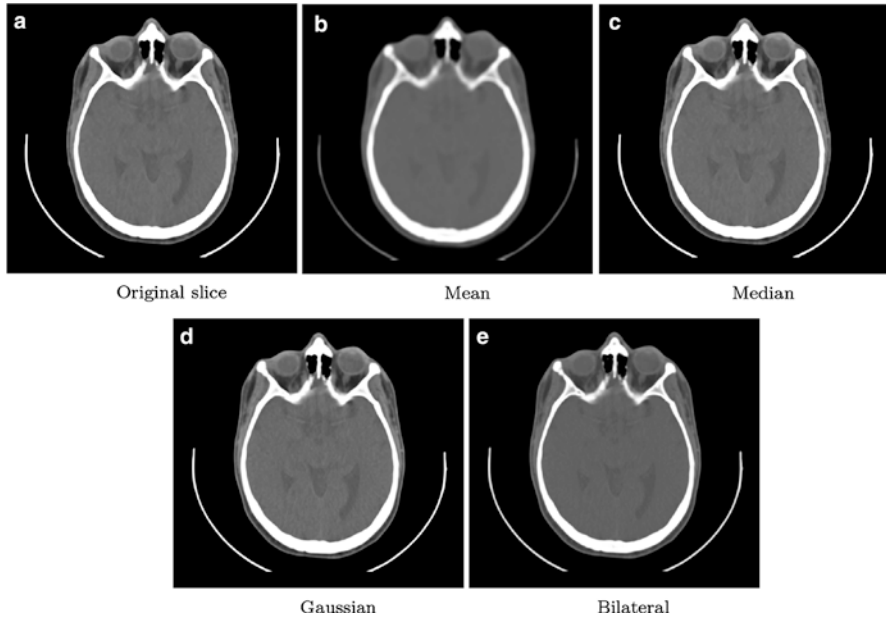


Fig. 5 Different techniques for image noise filtering

nonrepresentative values will have little impact on the median value. Furthermore, it can preserve sharp edges.

Gaussian filtering (Gonzalez and Woods 2002; Parker 2010; Russ 2015) is a smoothing operator that uses a Gaussian shape in the convolution process. In this filtering, the pixel or voxel values are replaced with weighted average of its neighbors following a Gaussian distribution.

Bilateral filtering (Tomasi and Manduchi 1998) is a smoothing technique that preserves image edges. Each pixel or voxel of the image is replaced with the weighted average of its neighbors, such that the weights take into account both spatial distances and intensity differences.

Figure 5 illustrates the application of smoothing filtering with mean, median, Gaussian, and bilateral filters to a given input image. The performance of noise filtering techniques varies according to the image modality. Quantitative and qualitative analysis studies have been reported in the literature (Andria et al. 2012; Manjón et al. 2008; Michailovich and Tannenbaum 2006; Salinas and Fernández 2007).

3.2 Edge Detection

Edge detection techniques (Gonzalez and Woods 2002; Parker 2010; Russ 2015) aim to identify boundaries between regions or objects through radiometric (intensity)

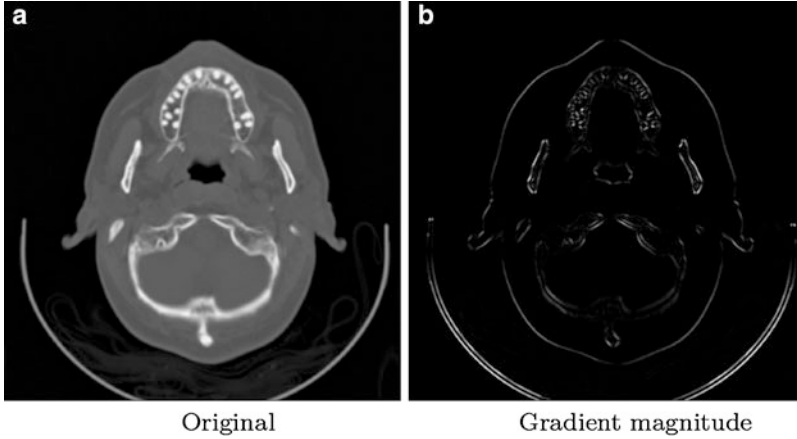


Fig. 6 Example of edge map obtained through gradient magnitude

discontinuities in the image. Pixels or voxels with sharp changes in brightness correspond to the edges of the image.

Most edge detection methods are based on the directional maxima of the gradient magnitude computed in a local neighborhood of each pixel in the image. The gradient direction is used to estimate the local orientation of the edges.

More formally, the gradient ∇f of an image f is expressed as

$$\nabla f = \left[\frac{\partial f}{\partial x}, \frac{\partial f}{\partial y} \right] \quad (2)$$

The edge strength corresponds to the gradient magnitude, given by

$$\|\nabla f\| = \sqrt{\left(\frac{\partial f}{\partial x}\right)^2 + \left(\frac{\partial f}{\partial y}\right)^2} \quad (3)$$

The gradient direction, perpendicular to the edge, is given by

$$\theta = \tan^{-1} \left(\frac{\partial f}{\partial y} / \frac{\partial f}{\partial x} \right) \quad (4)$$

Figure 6 shows an example of edge map calculated as the gradient magnitude in a neighborhood of each pixel in an input image.

The image gradient can be estimated by applying finite-difference approximations by applying first-order and second-order derivatives. Examples of edge detectors based on gradient information are Prewitt and Sobel (Gonzalez and Woods 2002), whose 3×3 kernels are expressed in Eqs. (5) and (6), respectively, expressed as

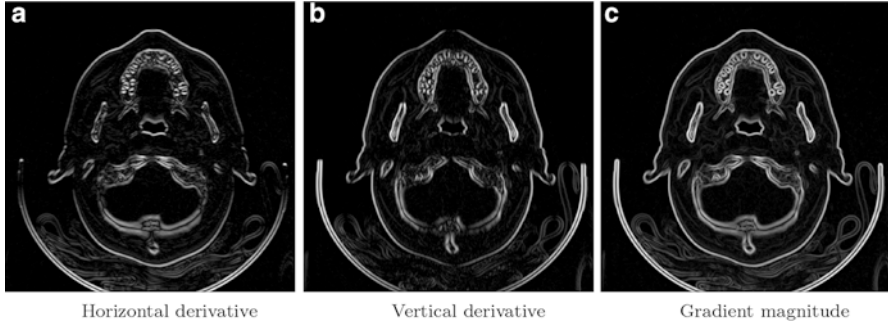


Fig. 7 Illustration of edge map computed through the Sobel operator

$$\frac{\partial f}{\partial x} \approx \begin{bmatrix} -1 & 0 & +1 \\ -1 & 0 & +1 \\ -1 & 0 & +1 \end{bmatrix} \quad \frac{\partial f}{\partial y} \approx \begin{bmatrix} -1 & -1 & -1 \\ 0 & 0 & 0 \\ +1 & +1 & +1 \end{bmatrix} \tag{5}$$

$$\frac{\partial f}{\partial x} \approx \begin{bmatrix} -1 & 0 & +1 \\ -2 & 0 & +2 \\ -1 & 0 & +1 \end{bmatrix} \quad \frac{\partial f}{\partial y} \approx \begin{bmatrix} -1 & -2 & -1 \\ 0 & 0 & 0 \\ +1 & +2 & +1 \end{bmatrix} \tag{6}$$

Figure 7 illustrates the results after applying Sobel operator to the image shown in Fig. 6a. Horizontal and vertical derivative approximations are computed and combined to generate the final edge map.

The Canny edge detector (Canny 1986) uses a Gaussian filter to initially smooth the image and attenuate noise. Then, the gradient is computed through a filtering such as Prewitt or Sobel, as mentioned previously. A nonmaximum suppression stage is used to maintain only the local maximum gradient values. This steps works as an edge thinning technique. Since the resulting edges can still contain pixels caused by noise or intensity variation, a double-threshold strategy is employed to remove spurious responses. Strong edge pixels correspond to those pixels with gradient value higher than the high threshold value, whereas weak edge pixels are those ones whose gradient value is smaller than the high threshold and larger than the low threshold. Pixels whose gradient value is smaller than the low threshold are suppressed. A hysteresis step is applied to keep the strong edge pixels while weak edge pixels can be connected to a strong edge pixel or removed according to its 8-neighborhood. Figure 8 illustrates the result after applying the Canny edge detector to the image shown in Fig. 6a.

3.3 Contrast Enhancement

Image enhancement techniques (Gonzalez and Woods 2002; Parker 2010; Russ 2015) have been developed to improve the quality of images for human interpretation purposes. Contrast is one of the most common aspects involved in the subjective

Fig. 8 Canny edge detector applied to an image

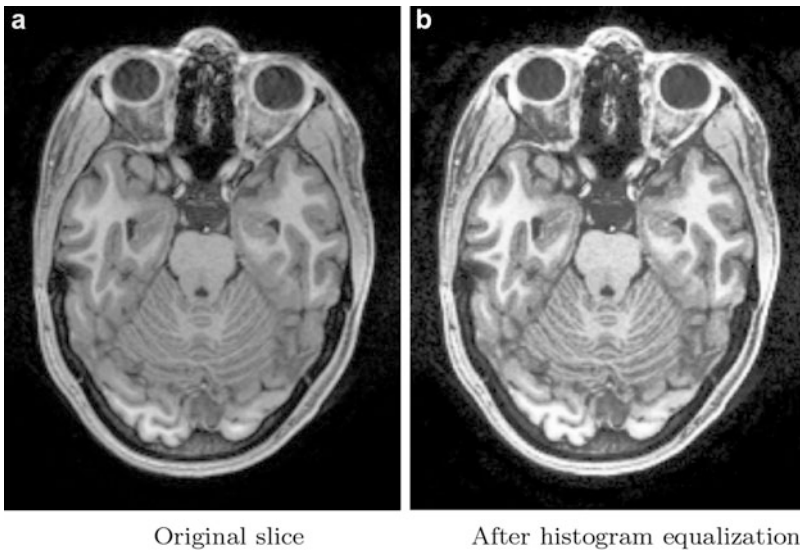


Fig. 9 Histogram equalization technique applied to an image

evaluation of image quality, which is measured as the difference in brightness or color between two adjacent regions.

Several contrast enhancement techniques (Kim et al. 1998; Singh and Bovis 2005; Stark 2000) use the image histogram to adjust its intensity values. An image histogram is a graphical representation of the number of pixels as a function of their intensity.

Examples of contrast enhancement approaches based on histograms include linear and nonlinear transformations. An important nonlinear technique is the histogram equalization, which redistributes the intensity values of pixels in the image such that the resulting image contains a uniform distribution of intensities. Figure 9 illustrates the result after applying histogram equalization to an image.

4 Segmentation

Image segmentation is the process of extracting objects or regions of interest from an image. This procedure is usually performed by applying a certain criterion to a range of intensity values, such as connectivity, similarity among others. An example of medical image segmentation is the selection of bone or a specific organ, such as heart or lung, for analysis and visualization purposes. Several methods have been proposed for image segmentation in the literature (Haralick and Shapiro 1985; Pal and Pal 1993; Zhang 1996). The following subsections present some relevant image segmentation techniques.

4.1 Thresholding

A common segmentation technique is known as thresholding (Sankur and Sezgin 2001), whose purpose is to identify an intensity value (grayscale or color) to separate objects from the background. Thresholding can find a global and unique threshold value for the entire image or a local and adaptive threshold for different regions of the image. For instance, considering an interval of values between t_{\min} and t_{\max} , pixel values outside this range could be set to 0, whereas pixel values within the interval could be assigned to 1. Let $f(x, y)$ and $g(x, y)$ be the input image and the resulting image after the thresholding process, respectively. Then,

$$g(x, y) = \begin{cases} 1 & \text{if } t_{\min} \leq f(x, y) \leq t_{\max} \\ 0 & \text{otherwise} \end{cases} \quad (7)$$

Global thresholding presents some drawbacks since it is sensitive to noise and dependent on the actual image intensity range. For instance, if the patient has a metallic material prosthesis, the global thresholding applied to a computerized tomography can produce artifacts due to the presence of noise with intensity similar to bone structures. In this case, adaptive local thresholding would be more effective.

4.2 Region Growing

The region growing technique (Adams and Bischof 1994) uses a seed located on the object or region of interest, which can be manually specified by the user or automatically assigned. Then, the seed expands gradually in accordance with its neighboring pixels. The expansion process interrupts when neighboring pixels satisfy a stopping criterion. Typical connectivity types for two-dimensional images are 4 and 8 connected neighborhood, whereas for three-dimensional images are 6-, 18-, and 26-connected neighborhood.

Stopping criteria are usually based on the homogeneity of the grayscale values or textural information present in the medical images.

4.3 Watershed

The watershed segmentation technique (Beucher 1994) is based on concepts of topography and hydrography, where an image is considered as a topographic surface, such that catchment basins are formed through a flooding process. The water follows the gradient of the image and flows along a path to reach a local minimum. At the end of the flooding process, the watershed of a relief corresponds to the limits defined by adjacent catchment basins.

An example of watershed segmentation applied to medical images is the separation of normal and abnormal tissues for detecting brain tumor in MR images.

5 Registration

Image registration (Brown 1992; Zitova and Flusser 2003) is the process of integrating two or more images into a common coordinate system. Medical image registration can be usually categorized into single-modality and multimodality approaches. Single-modality methods align images acquired by the same scanner type, whereas multimodality methods align images acquired by different sensor types, such CT and MR.

The registration process is useful for aligning data of a same patient captured at different view points or along different periods of time to monitor a treatment or the progress of a disease, such as a tumor growth.

Substantial research has been conducted on the image registration field over the last decades (Crum et al. 2014; Hill et al. 2001; Lester and Arridge 1999; Maintz and Viergever 1998). Several techniques have been developed to make the task successful with little or no human intervention, more precise, faster, and less sensitive to noise or occlusions.

Two stages are usually involved in the image registration: geometric and radiometric transformations. A geometric transformation maps spatial positions in one image to another, whereas a radiometric transformation maps intensity values in one image to another.

Geometric transformations perform basic operations such as resizing, translation, rotation, and projections. In addition to such rigid transformations, nonrigid or elastic transformation can also be applied to locally align one target image with a reference image. Examples of elastic transformations include the radial basis functions, which can be further categorized into other basis functions (Buhmann 2000), such as thin-plate spline, spline with tension, and multiquadric function.

Geometric transformations in the spatial domain aim to match features or intensity patterns in the images. On the other hand, frequency-domain geometric transformations explore invariance properties to simplify the location of correspondences between a pair of images. Peaks found in phase correlation methods through the fast Fourier transform (FFT) correspond to the relative translation between a pair of images. Differences under scaling and rotation can also be determined using log-polar coordinates and exploring Fourier transform properties.

Salient features, such as corners, edges and regions, can be detected from the images and used to match them. Common metrics used in the matching process include cross-correlation and mutual information.

6 Volume Rendering

Volume rendering can be defined as a set of techniques for displaying bidimensional projections from tridimensional data sets. These techniques can be categorized into two groups: *isosurface rendering* and *direct volume rendering*.

6.1 Isosurface Rendering

Isosurface rendering methods involve the extraction of an intermediary geometric representation from the volume data set. The most commonly used representation is the triangle mesh, which is formed by vertices and triangles that connect its vertices through edges. Figure 10 shows a triangle mesh and a magnified region to allow visualization of more details. Isosurfaces are useful to represent internal organs, bones, or other anatomic structures.

The technique of Marching Cubes (Lorensen and Cline 1987) is one of the most employed methods to generate isosurfaces, where a regular 3D grid, formed by cubes, overlaps the data volume, such that the vertices on the grid match the scalar values of the volume. Each cube edge is verified if it intercepts the surface. These intersections will be part of the isosurface vertices, which will be connected by triangles following one of 256 possibilities to form the surface. The final isosurface is generated by joining the surfaces from all cubes. However, the technique of Marching Cubes presents some ambiguities in some triangle configurations that

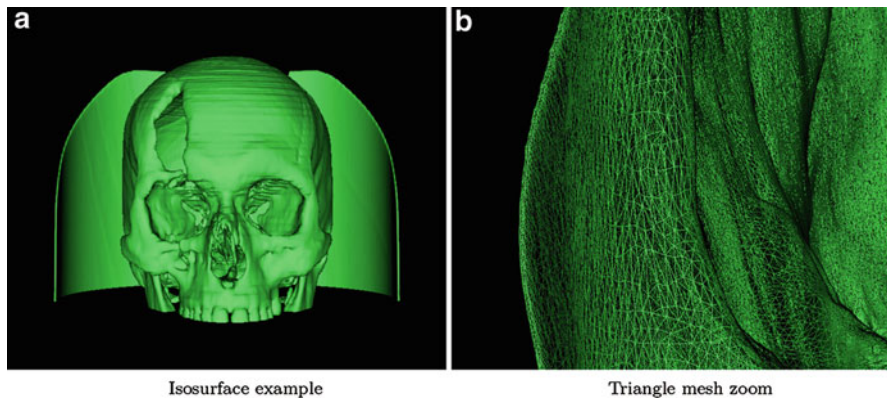


Fig. 10 Illustration of (a) an isosurface extracted from a volumetric medical data and (b) a magnified region of the mesh

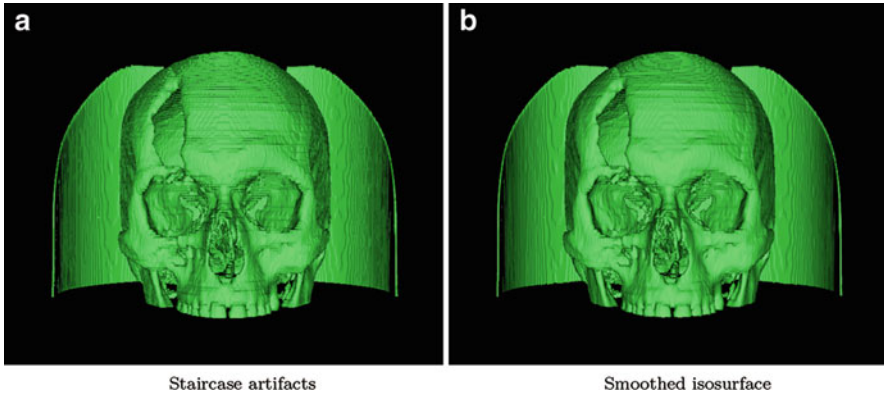


Fig. 11 (a) Isosurface with staircase artifacts and (b) same isosurface after the application of context aware smoothing algorithm to attenuate staircase artifacts

may generate holes in the isosurface. Other methods have been developed to avoid these problems, such as Marching Tetrahedra (Akio and Koide 1991) and Surface Nets (Gibson 1999).

Graphics processing units (GPUs) have been extensively used to process and display triangle meshes, as well as in 3D printing tasks. The triangle meshes can be used and edited in CAD tools to support surgical planning and prosthesis generation.

The quality of the isosurface depends on the methods used to generate it and on the segmentation process. Segmentation can generate a binary volume as result. Isosurfaces generated from binary volume usually present staircase artifacts, such as the ones shown in Fig. 11a. These artifacts are not natural to the patient's anatomy and they emerge mainly in high-curvature regions. Some techniques have been proposed to avoid these artifacts. The method developed by Whitaker (2000) smooths the binary volume toward the gradient direction to find the isosurface with minimum area. The context aware smoothing (Moench et al. 2011) method assigns high weighting coefficients to regions with occurrence of staircase while other regions have low weighting coefficients. The weighting coefficients control the degree of smoothing, such that high weighting coefficient areas are more smoothed. This is accomplished to reduce the loss of fine details in the resulting isosurface. Figure 11b shows the result after applying the context aware smoothing to a volumetric data.

6.2 Direct Volume Rendering

In direct volume rendering (DVR) (Roth 1982), the voxel values are mapped to colors and opacities according to a transfer function. Figure 12 illustrates an example of a transfer function. Color and opacity values are used to compose the final image according to the technique used. Volume ray casting (Levoy 1990) is one of the most common DVR techniques. In this technique, rays are traced from the observer,

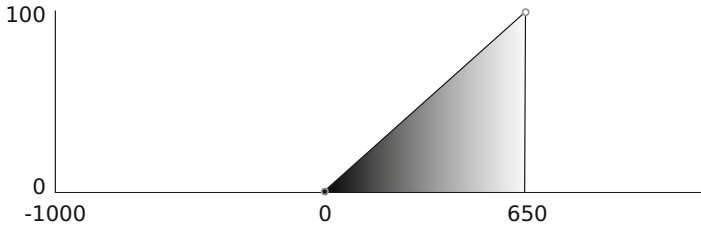


Fig. 12 Example of a linear transfer function, which maps scalar value 0 to black and 0% opacity. The scalar value 650 is mapped to white with 100%, whereas intermediate values are linearly interpolated to obtain color and opacity values

passing through an image plane, toward the object. The rays intercept the object voxels, such that the color and opacity values are accumulated to generate the final image. The emission-absorption (Fernando 2004) is an example of model to accumulate color and opacity values, expressed as

$$\begin{aligned}
 C &= \sum_{i=1}^n C_i \prod_{j=1}^{i-1} (1 - \alpha_j) \\
 \alpha &= 1 - \prod_{j=1}^n (1 - \alpha_j)
 \end{aligned}
 \tag{8}$$

where C and α are the accumulated color and opacity values computed iteratively, whereas C_i and α_i correspond to color and opacity, respectively, obtained from the segment i along the viewing ray.

In volume ray casting, structures of interest may be occluded by other structures. For instance, in a CT data set, soft tissues may occlude bones or regions due to contrast. However, it is possible to modify the transfer function, which can be done through user interaction or automatic methods for generating transfer functions. Figure 13 illustrates examples of volume ray casting applied to a volumetric data.

Maximum intensity projection (MIP) (Bruckner and Gröller 2009) addresses the problem of occlusion by taking into account the regions of interest with high scalar values. In MIP, the projection rays are not accumulated, instead the maximum scalar values are selected. One characteristic of MIP is its lack of visual depth information, which may lead to ambiguities in the visualization. MIP is useful to visualize bone structures, regions with different contrast, and tumors. Figure 14a illustrates an example of MIP rendering.

Minimum intensity projection (MinIP) (Mistelbauer et al. 2013) and average intensity projection (AIP) (Wu et al. 2008) are variations of MIP. In MinIP, the projection rays select the minimum values and can be used to provide information about blood flow deviation. In AIP, the projection rays show the mean value of scalar values obtained along their path. An example of AIP rendering is shown in Fig. 14b.

Maximum intensity difference accumulation (MIDA) (Bruckner and Gröller 2009) ponders the accumulation of color and opacity values along the rays through

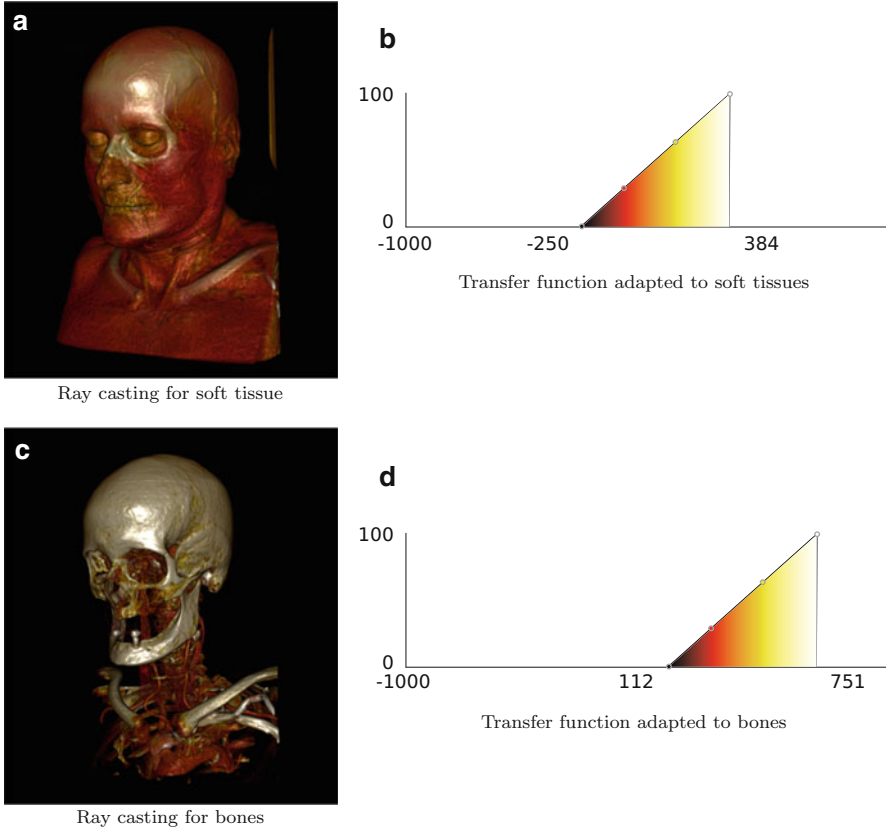


Fig. 13 Different views from ray casting for the same volume data set by modifying the transfer function. **(a)** the transfer function is adapted to reveal soft tissues; **(b)** the transfer function is modified to display bone structures

weights, which are calculated according to the maximum values intercepted along the ray path. The greater the difference between the maximum values, the higher the weights are assigned. Prioritizing the maximum values, MIDA can attenuate the problems associated with occlusion. Since MIDA uses accumulation, such as ray casting, the generated visualization presents depth information, which may reduce artifacts related to visualization ambiguities. Figure 14c shows an example of MIDA. Similar to MIP, MIDA is useful to visualize bone structures, regions with contrast, and tumors.

Contour MIP (Csèbfalvi et al. 2001) takes into account the angle between the viewing direction and the gradient vector from voxels intercepted by the projection rays, described as

$$s(P, V) = (1 - |(P) \cdot V|)^n \quad (9)$$

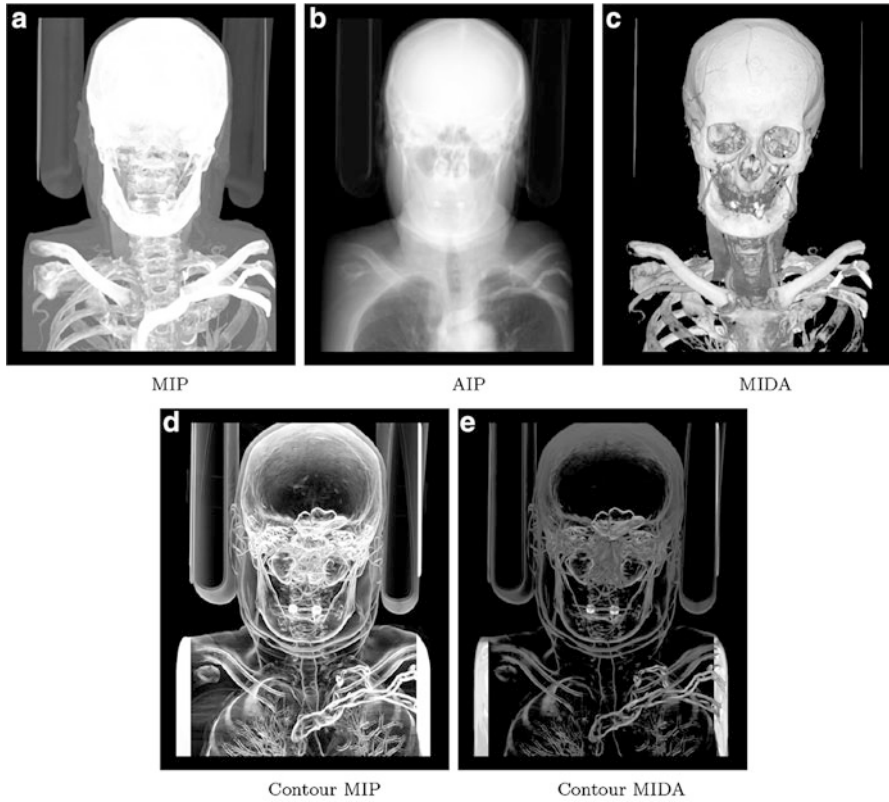


Fig. 14 A volume data set rendered through different volume rendering techniques

where $\nabla(P)$ is the gradient of voxel P , V is the viewing direction, and n is a sharpness coefficient for the contour. To compose the final image, contour MIP uses the MIP technique, since contour MIP may suffer from ambiguities in its visualization. Contour MIDA (de Moraes et al. 2015) follows the same idea as contour MIP; however, it uses MIDA to compose the final image to attenuate problems associated with ambiguities when compared to contour MIP. Both techniques emphasize voxels with higher values of gradient information, highlighting surfaces of different objects. Examples are illustrated in Fig. 14d and e.

7 3D Printing and Biofabrication

Nowadays, imaging is the basis for a series of applications that are already consolidate for a tailored treatment in medicine and odontology. Imaging is a noninvasive technique for human diagnosis and treatment. Therefore, a 3D model of an anatomy, generated from a patient CT or MRI medical scanner, can be integrated with additive

manufacturing (AM) technologies for many medical purposes. This is possible due to the concurrent development of scanning, imaging, and AM technologies. AM, also known as 3D printing or rapid prototyping, is based on the paradigm of a layer-by-layer automatically controlled deposition of materials by means of a myriad of processes. AM can produce directly a physical model from a virtual computational model and is considered a groundbreaking technology due to its flexibility and capacity to produce geometrically accurate complex models. A schematic diagram for 3D printing and additive manufacturing is illustrated in Fig. 15.

Imaging and AM technologies came to the market in the 1980s decade. Since then, a great evolution on both technologies and its integration for healthcare applications is paramount. Among them can be highlighted the production of 3D physical models, called biomodels, for a better and safer treatment, as well as the development of customized prostheses, medical devices, and surgical instruments (Silva et al. 2009; Sannomiya et al. 2008; Kemmoku et al. 2010; Oliveira et al. 2014; Giacomo et al. 2014).

Today's AM technologies use as a reference to print objects in a file format called STL (STereoLithography) created for the first machines in the 1980s decade by Albert Consulting Group under 3D Systems demand. This is a very simple representation of an object using triangle meshes to define all of its surfaces (internal and external). Each triangle is represented by means of three coordinates, one coordinate for each triangle vertex, and a normal vector pointing out of the object material, which allows to define the real boundaries of the object. The advantages of STL representation are mainly due to its easy interpretation from computing systems and cross-platform interoperability. To be used in AM, the STL file is sliced by means of parallel planes corresponding to the minimal layer thickness assured by the AM technology being used. The disadvantage is its redundant data representation composed of planar facets without any topological connectivity information. STL is still de facto standard for AM data exchange. The majority of the medical imaging software generate only STL format after all the steps explained in the previous sections of this chapter.

The AMF (Additive Manufacturing File Format) representation is an initiative of ASTM (American Society for Testing and Materials) since 2013 adopted by ISO (International Standardization Organization) as the international standard ISO/-ASTM 52915 (2013). The main idea of AMF is to overcome deficiencies and challenges of the STL file format, such as the independence among different AM technologies, represent geometry with colors, texture, multimaterials, and other properties, associated with the simplicity to be implemented and interpreted by computer systems. The adaptability to support part complexity and performance in terms of file size and processing is a desirable specification. AMF is also designed for compatibility with legacy systems (e.g., STL) and potential possibilities to be adapted for new demands for future technology evolutions. One important feature is the possibility to use not only flat triangles but also curved and surface triangles. AMF uses the XML (eXtensible Markup Language) as a standard to store and transport data readable for both human and computer.

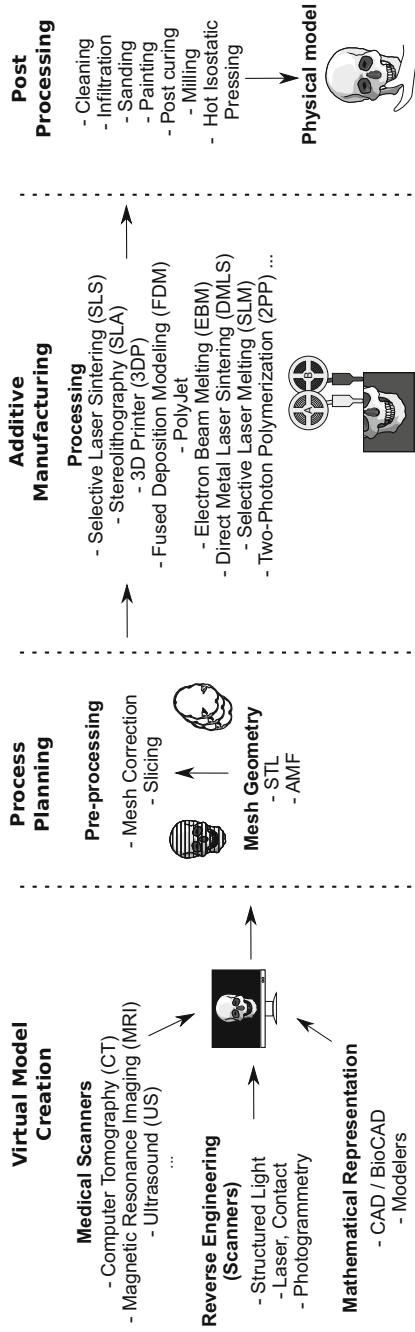


Fig. 15 3D printing and additive manufacturing techniques

Another 3D representation for AM is the 3MF (3D Manufacturing Format) file format. It is being developed by a joint development foundation project for creating the new file standard of AM. This project was originally created by some of the AM, CAD systems and software solutions providers such as Siemens, Dassault Systèmes, 3D Systems, Stratasys, SLM, HP, Materialise, Autodesk, Shapeways, NetFabb, and Microsoft. The 3MF format is developed under the philosophy of open-source. Similarly to STL and AMF, this format is a representation of an object composed of triangle element meshes. The proposal of 3MF is to promote a rich representation of an object in details, including colors, materials, and other characteristics. The 3MF will support extensions and innovations of the AM area, and interoperability among systems (3MF Consortium 2016b, c). It is expected for the consortium members a wide adoption. Its specification and codification can be found and downloaded from GitHub (3MF Consortium 2016a).

Looking toward biological directions of AM, imaging will play a fundamental role as a basis for the reverse engineering of organs and tissues anatomy. More recently, AM started to include biomaterials and biological materials as cells and microtissues as an option for printing. This is a new area called Biofabrication as rapidly growing field of research as a solution for the shortage of tissues and organs donation for restoration and replacement of human functionalities. Then, Biofabrication has appeared and grown in the last decade with many developments, potentials, and trials but also challenges.

Very recently, the term Biofabrication was reappraised by the 2010 created International Society of Biofabrication (ISB). Many novelties and developments obliged ISB to update the meaning of this wide word considering the derivations Bioprinting and Bioassembly. Then, the new ISB definition repositions Biofabrication as “the automated generation of biologically functional products with structural organization from living cells, bioactive molecules, biomaterials, cell aggregates such as micro-tissues, or hybrid cell-material constructs, through Bioprinting or Bioassembly and subsequent tissue maturation processes” (Groll et al. 2016). Three approaches as branches of Biofabrication have evolved: scaffold-based, solid-scaffold-free based on cell and tissue spheroids deposition, and a mix of them named as third strategy or hybrid technology (Rezende et al. 2012; Danilevicius et al. 2015).

The scaffold, as a first approach, consists of a three-dimensional structure as a temporary support for cells growing and maturing of a new tissue. The scaffold must be biodegradable, offering suitable conditions in such way the cells can be seeded and posteriorly adhere, differentiate, and proliferate for new tissue formation. Since AM allows for highly precise construction of 3D complex geometries and controlled porosity, scaffolds have been fabricated in many materials for different applications such as bone, cartilage, coronary, skin, and dental, among others. Reinforcing the role of controlled geometry of scaffolds with interconnectivity and therefore the guidance for the new tissue formation, many imaging techniques have been applied in order to verify the real scaffold's shape and geometry and to validate their applications. Noninvasive imaging techniques using CT and MRI have been researched to be used as a follow-up tool for an accurate assessment of bioresorbable

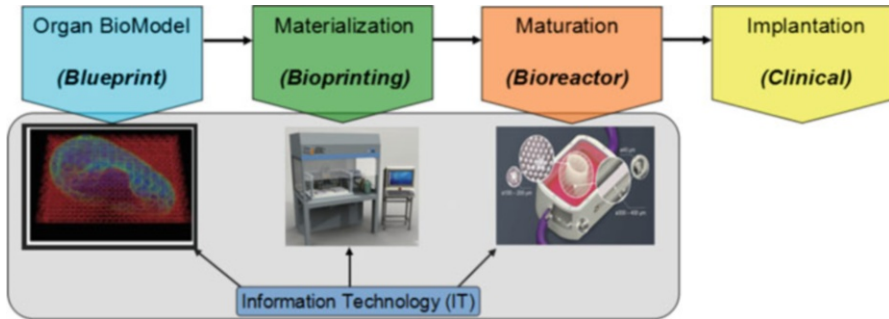


Fig. 16 Stages of bioprinting, from blueprint to clinical (Rezende et al. 2015; Murphy and Atala 2014)

vascular scaffolds (BVSs) after a percutaneous coronary intervention (Hickethier et al. 2016). Other authors have analyzed BVSs implanted in vivo by means of the optical frequency domain imaging (Naganuma et al. 2015). Even for scaffolds produced by conventional methods (non-AM), imaging has benefited the diagnosis of implanted scaffolds allowing for 3D quantification of parameters such as porosity, thickness, and surface area (Kłodowski et al. 2014).

In turn, solid-scaffold-free, based on cell or tissue spheroids controlled deposition, so-called Bioprinting or Organ Printing is defined as a layer-by-layer additive robotic computer-aided biofabrication of functional 3D organ constructs using self-assembling tissue spheroids according to a digital model or blueprint (Derby 2012; Melchels et al. 2012; Mironov et al. 2008; Rezende et al. 2015). On the other hand, Bioprinting is a dynamic strategy of biofabrication and is conceptually split into four stages: blueprint, materialization, maturation, and clinical application (Fig. 16). Each of these Biofabrication steps will, in the future, make use of imaging techniques for anatomical reverse engineering, mimicking and characterizing tissue micro and macro anatomic details, and also for quality control during maturation and clinical applications.

Different processes for bioprinting have been proposed (Atala and Yoo 2015), and they can be summarized as follows:

- **Inkjet Printing:** a noncontact printing technique that takes data from a computer representing an image or character, and reproduces it onto a substrate by ejecting tiny ink drops on a drop-on-demand manner (Mohebi and Evans 2002; Chua and Yeong 2014). Presorted cells are available in a 2D–printer cartridge-like. These cells are disposed drop-by-drop onto an $XY Z$ platform.
- **Scaffold-Free Printing:** this technique makes use of fluidity, where the fusion of the cell aggregates or cell rods are governed by the surface tension among two or more of those structures (Jakab et al. 2008). The live cells are encapsulated by some hydrogel, which assures mechanical protection and stability in order for the whole structure to become stronger. Thus, the cells can fuse to each other, generating the tissue and posteriorly the organ.

- **Extrusion-Based Deposition:** this technique uses a syringe for extrude the material under controlled pressure and temperature onto the platform. The material is normally at semi-melted condition which eases its deposition (Skardal et al. 2010). The materials are normally polymers or hydrogels and must be soft or fluid enough to facilitate extrusion through the small diameter tip or nozzle assuring mechanical strength itself after the deposition (Atala and Yoo 2015).
- **Laser-Induced Forward Transfer:** this technique utilizes a pulsed laser that is used to induce the transfer of material from a source film spread onto an optically transparent quartz support to a substrate in close proximity to or in contact with the film (Guillemot et al. 2010). This film is comprised of a printable material (biopolymer or protein) containing cells inside that are then deposited in a pattern on the substrate to create cellular structures and patterns. LIFT is supported on a transport layer, such as gold or titanium, which absorbs the laser energy and transfers it to the ribbon.

Bioprinting technology has a broad utility in various application areas, such as tissue engineering and regenerative medicine, transplantation and clinics, drug screening and high-throughput assays, and cancer research. Currently, a wide variety of tissues have been successfully bioprinted, such as thin or hollow tissues, for example, blood vessel, and tissues as such as bone, cardiac, cartilage, liver, lung, neural, pancreas, skin, and vascular (Ozbolat et al. 2016).

Image processing and computer graphics techniques for the creation of three-dimensional models or a blueprint for visualization and building of a complex organ are largely required. Therefore, for a bioprinting process the preprocessing includes data acquisition, printing model construction, printing path optimization, and materials preparation. Data acquisition refers to the process of obtaining anatomic geometries of the targeted tissues/organs and is usually implemented via medical imaging techniques, such as MRI and CT (Wu et al. 2017). So far, there is no sufficient knowledge to precisely define in which extent imaging will contribute for the Biofabrication field.

Medical imaging technology is an essential tool used by tissue engineers to provide information on 3D structure and function at the molecular, cellular, tissue, organ, and organism level. Computer-aided design/computer-aided manufacturing (CAD/ CAM) tools are also used to collect and digitize the complex tomographic and architectural information of the tissues. A comprehensive understanding of the composition and organization of the components that make up these tissues is the key requirement for reproducing the complex heterogeneous architectures that exist within functional tissues and organs (Murphy and Atala 2014).

For a complete blueprint, the most critical point is to obtain the best representation of human organs due to their complexity. For instance, replicating details of microvasculature of a 3D structure is hard task either from the anatomical or from mathematical and computational perspectives. Most of complex human organs are highly vascularized and have elaborated intraorgan branched vascular trees which dramatically increase the level of their structural organization and make task of designing corresponding organ blueprint more challenging (Rezende et al. 2015).

Furthermore, so far there is no software or model powerful enough to establish a blueprint.

Additionally, biomimicry and biomimetic are also considerable resources for the making-up of the blueprint, and they can be grouped in two main categories: those based on the use of imaging resources for the digitization of biological structures and those based on the use of mathematical and software resources for the construction of geometries with properties similar to those found in biological materials (Lantada 2016).

During the last decade, increasing attention has been paid for using fractals for promoting modeling, design, and simulation tasks in several areas of Biomedical Engineering, some of them also linked to the development of novel biomedical microdevices for interacting at a cellular and even molecular level. This includes modeling the behavior of microorganisms, complex organisms and their systems, scaffolds for tissue engineering, and the surfaces of organs and tissues (Lantada 2016).

In the conventional production systems, not only a product representation associated with user requirements and applications will not suffice. It is necessary to have available production lines and methods for fast, safe, and lean production of any product. As an analogy with this field, Biofabrication will face the same needs to be competitive when all the intermediate steps and associate challenges are overcome. Hence, a biofabrication line will be necessary with all the processes planning and execution needed.

A smart platform that enables real-time monitoring, informative decision-making, and automated operation will be necessary. Some key components include a data-driven interface, automated biofabrication line, efficient communication, and novel monitoring techniques customized for biomedical applications (Wu et al. 2017).

From an engineering point of view, the successful clinical translation of organ printing technology will depend not only on the development of a single tool or device, such as a robotic bioprinter, but rather on the entire complex of related technologies and their seamless integration, i.e., an Organ Biofabrication Line (OBL). The design and development of a fully integrated OBL, or development of a series of integrated automated robotic tools, is imperative for the future commercial translation of the organ printing technology (Mironov et al. 2011).

An organ biofabrication line will combine design, computer simulation, visual information of machines, devices, human resources and processes, as well as it must include *in silico* assays about tissue spheroids formation, spheroids fusion, cell viability, tissue and organ development in each corresponding stage. A virtual OBL must integrate essential tools such as CAD, CAE, CAM, complex mathematical modeling, and new specific software for biological simulations, special equipment and information technologies in general (Passamai et al. 2016).

Beyond the 3D representation available and in development today for AM, the Biofabrication field will need a complete new way to represent tissues and organs, based on its functionality, multimaterials composition, and micro/macro anatomic details. Imaging will play a fundamental role for this purpose. More comprehensive design systems need to be developed in order to integrate other crucial biological

factors into the process of building successful tissue constructs (Ozbolat and Gudapati 2016). A biofabrication line for organ production will be the next generation of production and, again, imaging will be necessary for characterization and quality control. Finally, new engineering tools associated with strong biological knowledge and translational methods will be necessary to support the biofabrication emerging area.

8 Conclusions

Continuous developments in medical image analysis have aided healthcare professionals in several diagnostic tasks. Technological advances in digital computing, medical imaging, biomaterials, and biofabrication have contributed to a broad range of medical applications. Critical diagnostic decisions have been improved by the integration of powerful computer-aided tools and manufacturing technologies.

In this chapter, we provided an overview of fundamental concepts related to the construction of three-dimensional models for visualization and biofabrication purposes. The understanding of such key topics is challenging due to the diverse and multidisciplinary field of biomedical engineering, however, of paramount importance to the development of innovative solutions to a variety of medical and health problems.

Acknowledgments We are grateful to São Paulo Research Foundation (FAPESP) for the Brazilian Research Institute for Neuroscience and Neurotechnology BRAINN (CEPID process 2013/07559-3) and for the Thematic Projects (Grants 2011/22749-8 and 2014/12236-1). We are thankful to Brazilian Council for Scientific and Technological Development (CNPq) for the Brazilian Institute of Biofabrication (INCT-BIOFABRIS process 2008/57860-3) and for the Regenerative Medicine grant (process 467643/2014-8) for the financial support. We also thank Otávio Henrique Junqueira Amorim for creating some of the illustrations and pictures.

References

- 3MF Consortium (2016a) 3MF materials and properties extension specification and reference guide. <https://github.com/3mfconsortium/>. Accessed May 2016
- 3MF Consortium (2016b) 3MF materials and properties extension specification and reference guide. http://3mf.io/wp-content/uploads/2015/04/3MFmaterialsSpec_1.0.1.pdf. Accessed May 2016
- 3MF Consortium (2016c) 3MF materials and properties extension specification and reference guide. http://3mf.io/wp-content/uploads/2015/04/3MFcoreSpec_1.0.1.pdf. Accessed May 2016
- Adams R, Bischof L (1994) Seeded region growing. *IEEE Trans Pattern Anal Mach Intell* 16 (6):641–647
- Akio D, Koide A (1991) An efficient method of triangulating equi-valued surfaces by using tetrahedral cells. *IEICE Trans Inf Syst* 74(1):214–224
- Amorim P, Moraes T, Silva J, Pedrini H (2015) InVesalius: an interactive rendering framework for health care support. In: Bebis G, Boyle R, Parvin B, Koracin D, Pavlidis I, Feris R, McGraw T, Elendt M, Kopper R, Ragan E, Ye Z, Weber G (eds) *Lecture notes in computer science*, vol 9474. Springer International Publishing, Switzerland, pp 45–54

- Andria G, Attivissimo F, Cavone G, Giaquinto N, Lanzolla A (2012) Linear filtering of 2-D wavelet coefficients for denoising ultrasound medical images. *Measurement* 45(7):1792–1800
- Atala A, Yoo JJ (2015) *Essentials of 3D biofabrication and translation*. Academic, London
- Beucher S (1994) Watershed, hierarchical segmentation and waterfall algorithm. In: *Mathematical morphology and its applications to image processing*. Springer, Dordrecht, Netherlands, pp 69–76
- Brown LG (1992) A survey of image registration techniques. *ACM Comput Surv* 24(4):325–376
- Bruckner S, Gröller ME (2009) Instant volume visualization using maximum intensity difference accumulation. *Comput Graphics Forum* 28(3):775–782
- Buhmann MD (2000) Radial basis functions. *Acta Numerica* 2000(9):1–38
- Canny J (1986) A computational approach to edge detection. *IEEE Trans Pattern Anal Mach Intell* 6:679–698
- Chua CK, Yeong WY (2014) *Bioprinting: principles and applications, vol 1*. World Scientific Publishing Co Inc., Singapore
- Crum WR, Hartkens T, Hill D (2014) Non-rigid image registration: theory and practice. *Br J Radiol* 77:S140–S153
- Csébfalvi B, Mroz L, Hauser H, König A, Gröller ME (2001) Fast visualization of object contours by non-photorealistic volume rendering. *Comput Graphics Forum* 20:452–460
- Danilevicius P, Rezende RA, Pereira FD, Selimis A, Kasyanov V, Noritomi PY, Silva JV, Chatziniakolaidou M, Farsari M, Mironov V (2015) Burr-like, laser-made 3D microscaffolds for tissue spheroid engagement. *Biointerphases* 10(2):021011
- de Moraes TF, Amorim PH, Silva JV, Pedrini H, Meurer MI (2015) Medical volume rendering based on gradient information. In: *Computational vision and medical image processing V: 5th ECCOMAS thematic conference on computational vision and medical image processing*, p 181, Tenerife, Spain. CRC Press
- Derby B (2012) Printing and prototyping of tissues and scaffolds. *Science* 338(6109):921–926
- Dowsett D, Kenny PA, Johnston RE (2006) *The physics of diagnostic imaging*. A Hodder Arnold Publication. Taylor & Francis
- Fernando R (2004) *GPU gems: programming techniques, tips and tricks for real-time graphics*. Pearson Higher Education, London
- Giacomo G, Silva J, Martines R, Ajzen S (2014) Computer-designed selective laser sintering surgical guide and immediate loading dental implants with definitive prosthesis in edentulous patient: a preliminary method. *European Journal of Dentistry* 8(1):100–106
- Gibson SFF (1999) Constrained elastic surfacenet: generating smooth models from binary segmented data. TR99 24. Mitsubishi Electric Research Laboratories, Inc., Cambridge
- Gonzalez RC, Woods RE (2002) *Digital image processing*. Prentice Hall, Inc., Upper Saddle River
- Groll J, Boland T, Blunk T, Burdick JA, Cho D-W, Dalton PD, Derby B, Forgacs G, Li Q, Mironov VA et al (2016) Biofabrication: reappraising the definition of an evolving field. *Biofabrication* 8(1)
- Guillemot F, Souquet A, Catros S, Guillotin B (2010) Laser-assisted cell printing: principle, physical parameters versus cell fate and perspectives in tissue engineering. *Nanomedicine* 5(3):507–515
- Haralick RM, Shapiro LG (1985) Image segmentation techniques. *Comput Vis Graphics Image Process* 29(1):100–132
- Hickethier T, Kröger JR, Von Spiczak J, Baessler B, Pfister R, Maintz D, Bunck AC, Michels G (2016) Non-invasive imaging of bioresorbable coronary scaffolds using CT and MRI: first in vitro experience. *Int J Cardiol* 206:101–106
- Hill DL, Batchelor PG, Holden M, Hawkes DJ (2001) Medical image registration. *Phys Med Biol* 46(3)
- Hsieh J (2003) *Computed tomography: principles, design, artifacts, and recent advances*. SPIE Press
- ISO/ASTM 52915 (2013) Standard specification for additive manufacturing file format (AMF). ASTM International, West Conshohocken
- Jakab K, Norotte C, Damon B, Marga F, Neagu A, Besch-Williford CL, Kachurin A, Church KH, Park H, Mironov V (2008) Tissue engineering by self-assembly of cells printed into topologically defined structures. *Tissue Eng A* 14(3):413–421
- Kapila S (2014) *Cone beam computed tomography in orthodontics: indications, insights, and innovations*. Wiley, New York

- Kelsey CA, Heintz PH, Chambers GD, Sandoval DJ, Paffett NLAKS (2013) *Radiation biology of medical imaging*. Wiley, Hoboken
- Kemmoku D, Noritomi P, Toland F, Silva J (2010) Use of BioCAD in the development of a growth compliant prosthetic device for cranioplasty of growing patients. In: *Innovative developments in design and manufacturing*. Taylor & Francis, London, pp 127–130
- Kim TK, Paik JK, Kang BS (1998) Contrast enhancement system using spatially adaptive histogram equalization with temporal filtering. *IEEE Trans Consum Electron* 44(1):82–87
- Kłodowski K, Nowicka K, Tarasiuk J, Wroński S, Świketek M, B-lazewicz M, Figiel H, Turek K, Szponder T (2014) Micro-imaging of implanted scaffolds using combined MRI and micro-CT. *Comput Med Imaging Graph* 38(6):458–468
- Lantada AD (2016) Microsystems for enhanced control of cell behavior. In: Lantada AD (ed) *Studies in mechanobiology, tissue engineering and biomaterials*, vol 18. Springer International Publishing, Berlin
- Leondes CT (2005) *Medical imaging systems technology: modalities, Medical imaging systems technology*. World Scientific, Hackensack
- Lester H, Arridge SR (1999) A survey of hierarchical non-linear medical image registration. *Pattern Recogn* 32(1):129–149
- Levoy M (1990) Efficient ray tracing of volume data. *ACM Trans Graph* 9(3):245–261
- Lorensen WE, Cline HE (1987) Marching cubes: a high resolution 3D surface construction algorithm. *Comput Graph* 21(4):163–169
- Lutz H, Buscarini E, W. H. Organization (2011) *Manual of diagnostic ultrasound*, vol 1. World Health Organization, Geneva
- Macovski A (1983) *Medical imaging systems*. Prentice Hall, Englewood Cliffs
- Maintz JA, Viergever MA (1998) A survey of medical image registration. *Med Image Anal* 2(1):1–36
- Manjón JV, Carbonell-Caballero J, Lull JJ, García-Martí G, Martí-Bonmatí L, Robles M (2008) MRI denoising using non-local means. *Med Image Anal* 12(4):514–523
- Melchels FP, Domingos MA, Klein TJ, Malda J, Bartolo PJ, Huttmacher DW (2012) Additive manufacturing of tissues and organs. *Prog Polym Sci* 37(8):1079–1104
- Michailovich OV, Tannenbaum A (2006) Despeckling of medical ultrasound images. *IEEE Trans Ultrason Ferroelectr Freq Control* 53(1):64–78
- Mironov V, Kasyanov V, Drake C, Markwald RR (2008) Organ printing: promises and challenges. *Regen Med* 3(1):93–103
- Mironov V, Kasyanov V, Markwald RR (2011) Organ printing: from bioprinter to organ biofabrication line. *Curr Opin Biotechnol* 22(5):667–673
- Mistelbauer G, Morar A, Varchola A, Schernthaner R, Baclija I, Köchl A, Kanitsar A, Bruckner S, Gröller E (2013) Vessel visualization using curvilinear feature aggregation. *Comput Graphics Forum* 32(3):231–240
- Moench T, Gasteiger R, Janiga G, Theisel H, Preim B (2011) Context-aware mesh smoothing for biomedical applications. *Comput Graph* 35(4):755–767
- Mohebi MM, Evans JR (2002) A drop-on-demand ink-jet printer for combinatorial libraries and functionally graded ceramics. *J Comb Chem* 4(4):267–274
- Murphy SV, Atala A (2014) 3D bioprinting of tissues and organs. *Nat Biotechnol* 32(8):773–785
- Naganuma T, Ishiguro H, Takagi K, Fujino Y, Mitomo S, Nakamura S, Nakamura S, Colombo A (2015) Provisional T-stenting with bioresorbable vascular scaffolds in vivo: insights from optical frequency domain imaging. *J Am Coll Cardiol Interv* 8(4):635–637
- Oliveira AT, Camilo AA, Bahia PRV, Carvalho ACP, Santos MF, Silva JVL, Monteiro AA (2014) A novel method for intraoral access to the superior head of the human lateral pterygoid muscle. *Biomed Res Int* 2014:1–8
- Oosterwijk H, Gihring P (2002) *Dicom basics*. OTech Inc, Aubrey
- Ozbolat I, Gudapati H (2016) A review on design for bioprinting. *Bioprinting* 3:1–14
- Ozbolat IT, Peng W, Ozbolat V (2016) Application areas of 3D bioprinting. *Drug Discov Today* 21(8):1257–1271

- Pal NR, Pal SK (1993) A review on image segmentation techniques. *Pattern Recogn* 26(9): 1277–1294
- Parker JR (2010) *Algorithms for image processing and computer vision*. Wiley, Indianapolis
- Passamai V, Dernowsek J, Nogueira J, Lara V, Vilalba F, Mironov V, Rezende R, Silva J (2016) From 3D bioprinters to a fully integrated organ biofabrication line. *J Phys Conf Ser* 705:012010
- Pianykh OS (2009) *Digital imaging and communications in medicine (DICOM): a practical introduction and survival Guide*. Springer, Berlin/Heidelberg
- Rezende RA, Pereira FD, Kasyanov V, Ovsianikov A, Torgensen J, Gruber P, Stampfl J, Brakke K, Nogueira JA, Mironov V, Silva JV (2012) Design, physical prototyping and initial characterization of ‘lockyballs’. *Virtual Phys Prototyping* 7(4):287–301
- Rezende RA, Kasyanov V, Mironov V, Silva JVL (2015) Organ printing as an information technology. *Procedia Eng* 110:151–158
- Roth SD (1982) Ray casting for modeling solids. *Comput Graphics Image Process* 18(2):109–144
- Russ JC (2015) *The image processing handbook*. CRC Press, New York
- Salinas HM, Fernández DC (2007) Comparison of PDE-based nonlinear diffusion approaches for image enhancement and denoising in optical coherence tomography. *IEEE Trans Med Imaging* 26(6):761–771
- Sankur B, Sezgin M (2001) Image thresholding techniques: a Survey over categories. *Pattern Recogn* 34(2):1573–1583
- Sannomiya EK, Silva JVL, Brito AA, Saez DM, Angelieri F, Silva Dalben G (2008) Surgical planning for resection of an ameloblastoma and reconstruction of the mandible using a selective laser sintering 3D biomodel. *Oral Surg Oral Med Oral Pathol Oral Radiol Endod* 106(1):36–40
- Silva J, Almeida A, Raposo do Amaral C, Ferreira D, Hotta L, Raposo do Amaral CA, Guidi M, Buzzo CL (2009) Three-dimensional virtual and physical technologies in the treatment of craniofacial anomalies. In: 11th international congress on cleft lip and palate related craniofacial anomalies, vol 1, pp 5–10, Bologna, Medmond Italy
- Singh S, Bovis K (2005) An evaluation of contrast enhancement techniques for mammographic breast masses. *IEEE Trans Inf Technol Biomed* 9(1):109–119
- Sistrom CL, McKay NL (2005) Costs, charges, and revenues for hospital diagnostic imaging procedures: differences by modality and hospital characteristics. *J Am Coll Radiol* 2(6): 511–519
- Skardal A, Zhang J, McCoard L, Xu X, Ottamasathien S, Prestwich GD (2010) Photocrosslinkable hyaluronan-gelatin hydrogels for two-step bioprinting. *Tissue Eng A* 16(8):2675–2685
- Stallings W (2005) *Data and computer communications*. Prentice Hall, Upper Saddle River
- Stark JA (2000) Adaptive image contrast enhancement using generalizations of histogram equalization. *IEEE Trans Image Process* 9(5):889–896
- Tomasi C, Manduchi R (1998) Bilateral filtering for gray and color images. In: Sixth international conference on computer vision, IEEE, pp 839–846
- Wahl RL, Wagner HN (2009) *Principles and practice of PET and PET/CT*. Lippincott Williams & Wilkins
- Whitaker RT (2000) Reducing aliasing artifacts in iso-surfaces of binary volumes. In: IEEE symposium on volume visualization, IEEE, pp 23–32
- Wu Q, Merchant F, Castleman KR (2008) *Microscope image processing*, 1st edn. Academic, Boston
- Wu C, Wang B, Zhang C, Wysk RA, Chen Y-W (2017) Bioprinting: an assessment based on manufacturing readiness levels. *Crit Rev Biotechnol* 37(3):333–354
- Zhang YJ (1996) A survey on evaluation methods for image segmentation. *Pattern Recogn* 29(8): 1335–1346
- Zitova B, Flusser J (2003) Image registration methods: a Survey. *Image Vis Comput* 21(11): 977–1000